Structural and dielectric anomalies near MPB region of $Na_{0.5}Bi_{0.5}TiO_3$-$SrTiO_3$ solid solution

Shahin Sayyed[1], Smita A Acharya[1], Pranay Kautkar[1], and Vasant Sathe[2]

[1]Department of Physics,RTM Nagpur University, Nagpur-440033, M.S. India
[2]UGC-DAE-CSR, University Campus, Khandwa Road, Indore 452001,India

In the present attempt, (1-x)NBT($Na_{0.5}Bi_{0.5}TiO_3$)-xST($SrTiO_3$) (x=0.24-0.28) solid solutions are studied near MPB region to investigate short range structural and dielectric anomalies. X-ray diffraction study confirms the presence of MPB by co-existence of rhombohedral (202), (122), and pseudocubic (002) (112) peaks at x = 0.25-0.26. For x = 0.24 absence of psedocubic peaks indicate the complete diffusion of cubic ST phase into the rhombohedral phase of pure NBT. RAMAN spectra exhibit appearance of new vibrational modes at A and B-site by splitting of bands in NBT-ST at MPB (x=0.25-0.26), which are not detected for x < 0.25 and x > 0.26. This can be assigned to local ordering at A-site cations (Bi/Na/Sr) and B-site TiO_6 octahedral distortion, respectively. The high temperature RAMAN spectra confirm the structural stability up to 550°C near MPB of all NBT-ST samples. Dielectric transition temperature is found shifted from 360°C to 160°C with ST and shows single broad anomaly. The broadening of dielectric peak with deviation from curie-weiss law proves dielectric dispersion near MPB region of NBT-ST. The origin of MPB is outcome of local imbalance due to chemical inhomogeneity at A-site and short range disordering at B-site. The induce strain-charge disparity influences dielectric behavior.

I. INTRODUCTION

$Na_{0.5}Bi_{0.5}TiO_3$ (NBT) is a perovskite-based complex ferroelectrics and found to exhibit morphotropic phase boundary (MPB) with the other perovskite such as $BaTiO_3$ (BT), $SrTiO_3$

S. Acharya: saha275@yahoo.com
Fax: (0712) 2500736

(ST) etc. Currently NBT-based perovskite are intensively focused as a next-generation of environmentally friendly lead-free piezoelectric material. Despite five decades of discovery of NBT and its derivatives, there is lack of clarity on certain crucial issues such as structural complexity, various aspects of atomic displacements and respective lattice distortions and their role in MPB. Basically, NBT is rhombohedral perovskite structure with R3c symmetry by polar cation displacements and antiphase rotations of oxygen octahedral **[1]**. The fundamental interest of the NBT-based solid solution is mixed-valency ions of very different electronic structure (e.g. Bi^{3+}, Na^{+}, Sr^{2+}, Ba^{2+}) sharing A site in perovskite. The local interaction between them during accommodation at the A sites give rise to series of concentration and temperature driven phase transition [2]. NBT has been found to exhibit different temperature driven phases such as rhombohedral, tetragonal and cubic with intermediate mixed phase between rhombohedral-tetragonal [3]. Concentration dependent structural transition of NBT-based solid solution is also very interesting. The room temperature phase diagram of (1-x)$Na_{0.5}Bi_{0.5}TiO_3$- x$BaTiO_3$ [NBT-BT] shows structural phase transition from rhombohedral to tetragonal with existence of rhombohedral-tetragonal MPB at x = 0.06 [4]. Whereas, for (1-x)$Na_{0.5}Bi_{0.5}TiO_3$- x$SrTiO_3$ [NBT-ST], rhombohedral to cubic phase transition has been observed with increasing Sr concentration with rhombohedral- cubic MPB [5-8].The exact concentration of ST in NBT for MPB is not clear. The role of BT or ST specially A-site ions in formation of MPB in NBT is needed to be closely monitored to understand the origin. The existence of exact location of MPB, role of different ions at A and B site, local disorder and lattice displacement in most of the solid solution are inconclusive.[5-8]

There are many recent attempts to probe structural anomalies in NBT-based materials near MPB. Gorfman et al have studied the low symmetry phase in $NaBiTiO_3$ crystal by using

Optical Birefringes Microscopy and predicted that below 573 K, $NaBiTiO_3$ sustained monoclinic structure instead of Rhombohedral [9]. Trujillo et al have observed pressure induced phase transition in NBT-based system $(Na_{0.5}Bi_{0.5})_{0.89}Ba_{0.11}TiO_3$ by using RAMAN spectroscopy and found phase transition in sequence of tetragonal → rhombohedral → cubic with increasing pressure [10]. Rout et al have detected MPB in Ba doped $Na_{0.5}Bi_{0.5}TiO_3$ by using high temperature RAMAN and X-ray techniques [11].

Dielectric behaviour of NBT-based system has been found very sensitive to temperature and dopant level. First dielectric anomaly has been reported at ~ 220°C named as 'T_d' representing ferroelectric to antiferroelectric phase transition. The second dielectric anomaly has been observed at ~320°C abbreviated as 'T_m' corresponding with rhombohedral to tetragonal structural transition [12-14]. Many research efforts have been intended to correlate the structural transition and dielectric anomaly [15-18]. In order to understand the phase transition anomalies in this system, solid solutions such as $0.94Na_{0.5}Bi_{0.5}TiO_3$-$0.06BaTiO_3$[19] $Na_{0.5}Bi_{0.5}TiO_3$-$Bi_{0.5}Li_{0.5}TiO_3$, $Na_{0.5}Bi_{0.5}TiO_3$-$Bi_{0.5}K_{0.5}TiO_3$[20], $Na_{0.5}Bi_{0.5}TiO_3$-$CaTiO_3$[21], $(NaK)_{0.5}Bi_{0.5}TiO_3$[22], $Na_{0.5}Bi_{0.5}TiO_3$-$K_{0.5}Na_{0.5}NbO_3$[23], $Na_{0.5}Bi_{0.5}TiO_3$-$BaTiO_3$-$K_{0.5}Na_{0.5}NbO_3$[24], $Na_{0.5}Bi_{0.5}TiO_3$-$SrTiO_3$ [25] etc have been developed. Formation of MPB in NBT-based solid solution is found responsible to tune phase transition and enhanced electromechanical properties.

To understand the origin of MPB, chemical homogeneity and respective short range structural changes near MPB is needed to be monitored closely. RAMAN Spectroscopy is widely used to probe the short range structural changes [26, 27, 24]. In spite of many studies, several important questions like (i) A-site atomic ordering for different cations and their influences on association with B and O ions, (ii) The effect of the local interaction on symmetry and structural changes are still needed to be enlightened.

In the present attempt, nanosize NBT-ST solid solution at composition x = 0 - 0.30 were synthesized by using novel hydrothermal combustion route. The compositions of ST(x) were finely varied by 0.01 intervals to exactly locate ST content at MPB. According to our knowledge, this is first attempt to prepare fine-scale NBT-ST by this synthesis route. X- ray diffraction (XRD) data are used to confirm the crystalline pure phase structure of the NBT-ST solid solution. The composition and temperature dependent short range structural transition and dielectric behavior are closely monitored near MPB. Local structural disorderings are studied by Raman Spectroscopy. Existence of MPB are confirmed by the development of new shoulders in XRD peaks, which outset at x = 0.25 and disappear at 0.27 onwards. It clearly indicates that below this composition material well exhibit rhombohedral symmetry and above it transform to pseudocubic structure. RAMAN spectra show additional vibrational modes i) at A-site by splitting of the broad band around 100 cm^{-1}, which are associated with Bi-O, Sr-O, Na-O respectively, (ii) at B-site by splitting of band around ~276 cm^{-1} related to TiO_6 octahedral distortion at MPB region (x = 0.25 -0.26) in NBT-ST solid solution A small shoulder is observed around 670 cm^{-1} corresponding with Ti-O stretching mode which is found disappears at x= 0.27 onwards and (iii) high temperature Raman spectroscopy exhibits anomalous vibrational modes at B-site around 140^{o}C. These can be associated to dielectric transition, which is around ~160 ^{o}C and related with antiferroelectric to paraelectric phase transition. The dielectric transition temperature is found reduced from 320^{o}C to 160 ^{o}C.

II. EXPERIMENTAL PROCEDURE

In present work we have synthesized the (1-x) NBT-x ST (x = 0, 0.24, 0.25, 0.26, 0.27, 0.28) solid solution by using a novel hydrothermal combustion method. The precursors were taken in the form of nitrate. Bismuth Nitrate ($BiNO_3.5H_2O$, Sigma Aldrich), Sodium Nitrate ($NaNO_3$, Merck), Strontium Nitrate ($SrNO_3$, Sigma Aldrich) and Titanium Isopropoxide ($Ti(OC_3H_7)_4$, Across) were used as an starting precursors. Nitric acid (HNO_3) was used as a solvent and Liquor ammonia (NH_4OH) was used for adjusting the pH of the solution. Citric acid was used as a chelating agent as well as fuel for combustion method. The synthesis was carried out in two steps. First a separate solution of Titanium Isopropoxide was prepared in citric acid with molar ratio of metal cation to citric acid 1:2. The pH of the solution was made to ~ 6 by adding liquor ammonia drop wise. Then the stoichiometric amount of Titanium isopropxide was added and stirred at 80^{o}C for 2 hours. Secondly all the metal nitrates were dissolved in nitric acid. Then the citric acid with a molar ratio of metals to citric acid 1:2 was added into it. The liquor ammonia was added to maintain the pH of the solution to ~ 6. After that the solution of the titanium was added and the total solution was stirred for 20 minutes at room temperature. The solution was then transferred to Teflon line steel autoclave of capacity 300 ml. The autoclave was placed in hot air oven at temperature 120^{o}C for 30 hours. Then the autoclave was allowed to cool naturally. The resulting solution was transferred in a glass beaker and heated at 220^{o}C in a open muffle furnace. This process was leading to evaporation followed by exothermic chemical reactions that result in a production of flames. The resulting powder was calcined at 700 ^{o}C for 3 hours in a programmable closed muffle furnace with a heating rate of 5^{o}C/minute to obtain a well crystalline NBT-ST powder. The resulting powder is grind in agate mortar by adding 2 % polyvinyl alcohol as a binder. The powder was poured in a 9 mm steel die punch to form a pellet under the pressure of 7 Mpa for 15 minutes in a hydraulic press. The pellets were sintered in a programmable muffle furnace at different temperature (800 to 950^{o}C) for 4 hours to optimize the sinterability. The relative density of all pellets was obtained in between 92 to 94%.

The crystal structures of the resulting calcined powder were characterized by X-ray Powder diffraction using D8 Advance Bruker Germany 2.2 KW Cu anode and Ceramic X-ray tube. The data were recorded with a step size 0.197 and step time 46.5 ms. Electronic microscope images and EDX of the samples were performed by using JEOL/EO, JSM-6380 electron microscope. RAMAN Spectra were recorded in the temperature range 50^{o}C to 550^{o}C within the wavenumber range 50 cm^{-1} to 1000 cm^{-1} by Jobin Horibra LABRAM-HR visible. The samples were excited by the Laser source-He-Ne 632.8 nm and Argon 488 nm. For electrical properties, the silver paint was applied on the surface of the pellet. To form a good electrical contact the pellet was dried at 500^{o}C for half an hour in a closed muffle furnace. The dielectric measurement in a temperature range 30-500^{o}C were done on a LCR meter (model 4100 Waynkerr) equipped with a programmable box furnace with heating rate of 2^{o}C/min.

III. RESULT AND DISCUSSION

A. X-ray diffraction

X-Ray Diffraction patterns of the (1-x) NBT-xST (x = 0, 0.24-0.28) are shown (FIG. 1) (a, b and c). The XRD data for x=0.24 are well fitted by Rietveld refinement done (see FIG.2) by using R3c space group and with Pseudo voigt function confirms the single phase pure rhombohedral perovskite structure. However, for x =0.25, an additional shoulder are detected near the peaks 2θ = 46.8 (202) and 2θ = 58.2 (122) and found to be related with (002) and (112) of cubic phase of NBT. The presence of (202), (002), (122) and (112) peaks represent the co-existence of rhombohedral and pseudocubic phase (FIG 1b,c). To get more clarity to this observation XRD peak at (202) is fitted by Guassian function (see FIG 3). It confirms the origin of shoulder with shifting of (202) peak towards higher angular side at x = 0.25. The shoulder peak is related to (002) of pseudocubic phase of BNT-ST. It gives clear evidence for formation of Morphotropic Phase Boundary, which is beginning at x = 0.25 and continue and more prominent for x = 0.26. Whereas, for the composition x = 0.27, the (202) and (122) peaks suddenly disappear and structure are found to match with pseudocubic structure. Thus the variations of composition concentration from 0.24 to 0.28 in NBT-ST are found to induce structural transformation from rhombohedral to pseudocubic mediated by rhombohedral-pseudocubic MPB. The accompanied lattice parameters shift as a function of ST content were calculated from the diffraction peaks based on the rhombohedral (R3c) space group (shown in the inset of FIG 1a). a/c→~1 (x>0.26) with composition is clear evidence for the decrease in rhombohedral phase and emergence of pseudocubic structural transition.

Tolerance factor plays a more essential role on the phase transition of the system. Goldsmith Tolerance factor [28,29,30] given by the equation $t = \frac{R_A + R_o}{\sqrt{2}(R_B + R_O}$ where R_A, R_B and R_0 are the radii of the A and B ions and oxygen ions respectively are used for explaining the structural transformation in perovskite materials. The addition of ST into the NBT slightly increases the tolerance factor of the NBT-ST solid solution because of the larger tolerance factor of ST(1.013) than that of the pure NBT (0.977) which indicates that the rhombohedral structure of the NBT are deviated to more symmetric ideal cubic perovskite at higher concentration of ST.

B. Electronic microscopy image and EDX result

Figure 4 a and b shows the Electronic microscopy image and EDX result of calcined powder of $Bi_{0.5}Na_{0.5}TiO_3$ and $0.74(Bi_{0.5}Na_{0.5}TiO_3)$-$0.26(SrTiO_3)$ ceramics, respectively. Both the SEM images reveal highly agglomerated irregular shape particles having size below 100 nm.

This is always expected in combustion synthesized samples. The element distributions in NBT and NBT-ST are checked by EDX, see Fig 5 a and b, respectively. EDX results exhibits existence of all elements with appropriate concentration except slight change in Bi and Na proportion as compared to expected stoichiometry 1:1. This can be attributed to loss of Bi due to high volatile nature. EDX data for both the samples are listed in table 1. The additional element Cu, Au, Pd is due to coating, Si due to glass substrate and C due to atmosphere.

C. Raman spectroscopy

Room Temperature RAMAN Spectra of the unpoled (1-x)NBT-xST (x=0,0.24-0.28) are studied and displayed in FIG 6. All the peaks are fitted by Lorentzian function. Insight of FIG 6 shows Lorentzian fitted data file of 0.76NBT-0.24ST (sample system). As the room temperature crystal structure of the end members of the NBT-ST solid solution has been reported as Rhombohedral R3c for NBT and Cubic pm-3m for ST. For the composition in neighborhood of MPB generally presence of both the phases has been reported. According to the group theory given by Kreisel etal [31], there are 13 IR and RAMAN (7A1+6E) active modes for BNT R3c structure. The simultaneous IR and RAMAN activity produces the splitting of each A1 and E mode into their longitudinal and transverse optic mode so that in principal 24 mode should be visible in RAMAN spectra of R3c structure. However the intensity of some of this mode is very weak and in pure NBT, it causes broadening of the neighboring band. Hence in the RAMAN spectra of pure NBT, 4 broad peaks have been reported by Parija etal [32]. These are assigned as:(i) band centered at 146 cm^{-1} $A_1(TO_1)$ related to the distorted octahedral BiO_6 and NaO_6 cluster. (ii) Broad band near 281 cm^{-1} E (TO_2) due to stretching of short range TiO_6 octahedral. (iii) Band at 542 cm^{-1} (LO_2) attributed to O-Ti-O stretching symmetric vibration of the TiO_6 cluster. (iv) Broad band centered at 812 cm^{-1} (LO_3) mode has been assigned to longitudinal

(LO) and transverse (TO) components, which are due to presence of the sites containing octahedral distorted [TiO_6] clusters in the rhombohedral lattice. However, for ST cubic structure no first order RAMAN active modes are generally obtained. It shows second order RAMAN scattering peaks in the room temperature RAMAN Spectrum. Moreover, two peaks in the range 200-500 cm^{-1} and in between 550-750 cm^{-1} has been detected in the room temperature RAMAN spectra of bulk cubic ST [33].

Our results show the red-shifting in the Raman peaks of NBT-ST in comparison to literature can be assigned to the particle size effect. The dominant features of RAMAN spectra: (i) peaks are observed near ~70 cm^{-1}, 110 cm^{-1}, ~134 cm^{-1}, ~274 cm^{-1}, and ~540 cm^{-1}, while broad and weak band at ~810 cm^{-1}, (ii) weakening of mode near 134 cm^{-1} and completely disappears x = 0.27, (iii) splitting of mode near 274 cm^{-1} for x = 0.25 and 0.26 (iv) hardening of mode near 540 and anomalous at x = 0.25 onwards. (v) Weak peak at 620 cm^{-1} and disappears at x = 0.27 onwards (vi) splitting of mode near 840 cm^{-1} for x = 0.26. These changes can be seen more clearly in the inset of FIG 4, determined by fitting the spectra by Lorentzian lines. The splitting of modes and discontinuity in frequencies change at x = 0.25 and 0.26 are evidences of local structural rearrangement.

The vibrational mode near 70 cm^{-1}, 110 cm^{-1} and 138 cm^{-1} can be assigned to A-site cations vibration of BiO_6, SrO_{12}, NaO_6 cluster respectively in accordance to mass frequency relation. The magnified view of composition dependent A-site cations vibrations of NBT-ST (FIG 6) shows: (i) For x = 0 and x = 0.24, weak A-site modes associated with vibration of BiO_6 and NaO_6 cluster are detected. (ii) For x = 0.25 and 0.26, the clear and distinct features of all three A-sites vibrational modes are clearly observable and attributed to local ordering of Bi, Na and Sr ions at A-site~~.~~ (iii) However, for x = 0.27 onwards, mode related to vibration of NaO_6

cluster is suddenly disappeared; indicates Na disordering at A-site may be due to Sr. Local interaction between Na and Sr are more probable; due to close similarity of Na and Sr as Na-O and Sr-O bond have ionic nature, while the Bi-O is highly covalent and Bi is volatile. All these lead to the disordering of Sr/Na at A-site during rearrangement. For $x < 0.25$, material shows rhombohedral phase of NBT. However for x=0.25 and 0.26, all cations local ordering leads to co-existence of rhombohedral-pseudocubic phases. For x=0.27 onwards, Na disordering at A-site come up with pseudocubic phase.

Close look of B-site vibrational mode shows that broad band near 274 cm^{-1} corresponding with Ti-O vibration in TiO_6 octahedra are splitted into sharp peaks at the MPB region. However for x<= 0.27 the bands resolved into single broad peaks. The splitting can be assigned to asymmetric vibrations of Ti-O bonds and thus TiO_6 octahedral distortion induces non-uniform Ti-cation displacements, which are prominent at MPB region in NBT-ST. Similarly the mode near 542 cm^{-1} (FIG 4) associated with O-Ti-O stretching symmetric vibration of the TiO_6 cluster is harden with rising ST concentration and becomes anomalous at MPB. A shoulder is detected near 680 cm^{-1} for x = 0.24 to 0.26 and disappear at x = 0.27 onwards. The broad and weak band centered at 812 cm^{-1} (LO_3) mode is commonly associated with distorted sites arises due to presence of the octahedral distorted [TiO_6] clusters in the rhombohedral lattice. The polar character of lattice classify this mode into longitudinal (LO) and transverse (TO) component. An anomalous split in the mode is detected at x = 0.26.

All these spectral changes reveal that for ST concentration x= 0.25 and x= 0.26 ordering of Bi, Na, ST at A-site are clearly viewed with sharp splitting of B-site peak. It attributes to structure and symmetry shift at x=0.25 and x=0.26. The cations (Bi^{3+}/Na^{1+}/Sr^{2+}) ordering at A-site and Ti-displacement by TiO_6 octahedral distortion at B site outset at x=0.25 are responsible for co-existence of rhombohedral-pseudocubic phase at MPB. The disordering of Na^+ at A-site and symmetric Ti-O vibration in TiO_6 octahedra at B-site observed at x = 0.27 is leaded to structural transition from MPB to pseudocubic as replicated by XRD profile (FIG.1).

According to symmetry and selection rule of NBT and ST, a gradual change from rhombohedral to cubic can be expected with increasing Sr concentration which can lead to a decrease in Raman active mode. The existence of almost all Raman modes associated with rhombohedral phase and XRD peaks matched with cubic phase for $x \geq 0.27$ indicates gradual transition of rhombohedral to pseudocubic through intermediate short range non-cubic phases.

The temperature dependent Raman vibration and respective short range structural changes of NBT-ST system near MPB are monitored by high temperatures RAMAN spectroscopy (see FIG 7). The irreversibility of the local changes is also investigated by studying the spectra during cooling (see FIG 7). The five different compositions (x = 0.24, 0.25, 0.26, 0.27, 0.28) of the unpoled (1-x) NBT-xST solid solution very close to MPB regions are probed for temperature range 30 to 550^{o}C during heating and cooling cycle. The temperature driven spectral anomalies which are commonly observed in all compositions are (i) broadening of mode with reduction of FWHM, (ii) decreasing of intensity of peaks with rising temperature and (iii) asymmetric peaks. The trend is reproduced during cooling (see FIG 7). All these attributed to temperature induced local structural disordering and excitation of additional vibrational modes near local structural heterogeneity, respectively. No any prominent vibrational modes are detected in the given temperature range (30 – 550^{0}C). However some new modes at A-site and B-site are noticed for x=0.26 and 0.27. These are not found to be reproducing during cooling. The temperature sensitive Raman vibration have not shown any bulk structural transition up to 550^{o}C; indicates MPB region is also sustained up to 550^{0}C.

The origin of MPB lies in the disorder of the Bi^{3+}, Na^{+} due to insertion of Sr^{2+} ions at A-site and resultant Ti- displacement at B-site in ABO_3 perovskite. The divergent nature of bonds Sr-O, Na-O and Bi-O are responsible to induce A-site local disordering. The Na-O and Sr-O are ionic, the Bi-O is highly covalent according to Pauli scale. The divergence of bondings is anticipated by introducing positional disorder on the oxygen sublattice. The rising of Sr-O concentration is responsible to increase the disordering. As O cloud is distributed to form A-O and B-O bonds in ABO_3 perovskite. The A-site induces positional distortion in oxygen sublattice leads to Ti-O bond deformation, which is accompanied by TiO_6 octahedral distortion and Ti-displacement.

III.C Dielectric study

The temperature and frequency dependence of the dielectric behaviour of unpoled (1-x NBT-xST) sample at 10 KHz, 100 KHz and 199 KHz in the temperature range 30°C to 400°C are investigated (see FIG 8). The dielectric permittivity as a function of temperature (έ-T curve) of pure NBT exhibits anomaly around 320°C; can be associated to structural transition from room temperature rhombohedral to tetragonal phase. However, the T_d (depolarization Temperature) corresponding with the polar ferroelectric to antiferroelectric transition is not detected; it may be suppressed due to unpoled nature of the sample. Dielectric constant is found continuously rising with temperature 550°C which is related to tetragonal to cubic transition in case of pure NBT.

In NBT-ST solid solution near MPB region έ-T curve displays dielectric anomaly around 160°C (see FIG 8). The central broad peak observed for each composition correlates to antiferroelectric (non centrosymmetric space group: R3c) to paraelectric phase transition (non centro symmetric space group: P4mm) transition. It is evident that doping induces two major changes in the NBT system (i) shifting the peak temperature (T_m) to lower temperature, and (ii) the broadening in the dielectric spectra. Lowering of transition temperature with ST concentration can be attributed to increase in isovalency of NBT-ST solid solution at A-site by partial replacement of ($Bi^{3+}Na^{1+}$) by Sr^{2+} and covalency of A-O bond with fractional replacement of Na-O by Sr-O with rising ST concentration [25]. As Na-O bond and Sr-O bond has ionic nature, while Bi-O bond have covalent nature as discussed earlier. Thus shift in valence state of A-site and covalency of A-O bonds induces polarization anomaly in the structure which leads to lowering of the transition temperature. Also it has been observed that ferroelectricity in NBT is originated due to the lone pair effect of Bi^{3+} and the partial replacement of Sr^{2+} at the A site could affect to decrease the T_m value [33].

The broadening of ε-T curve is consequence of strain and disordering induced relaxation polarization near transition temperature. The dispersions in the dielectric can also be explained by the strong heterogeneity induced at the A site due to the partial replacement of Bi^{3+} and Na^{1+} by Sr^{2+} which perturb the coulomb interaction at long range and shows the formation of polar nano domains. The heterogeneity in the random field lattice may decrease the degree of coupling between permanent dipoles [34]. Therefore the ferroelectric domains are destroyed and the short range cation ordering resulting in a polar nano are formed which include the relaxor ferroelectric behavior [35]. The frequency dispersion is also detected in the frequency range 10-200 KHz. For three different frequencies (10 KHz, 100KHz and 199KHz) έ-T curves are distinguishable and demonstrated compositionally disordered system such as relaxors. However, the sample with composition x = 0.24 show weak frequency dispersion and relaxation before phase transition as well as lower dielectric loss. For the composition x = 0.26 and 0.27 sudden rise in dielectric loss are observed for temperature around $300^{o}C$. This attributes to conductance due to mobile charge carriers.

The fall of the dielectric constant after the transition temperature in a normal ferroelectric material generally follows Curie-Weiss law. The behavior is demonstrated by plotting 1/έ as a function of temperature at constant frequency 100 KHz for different compositions (FIG 9). The high frequency is chosen to eliminate the effect of interfacial capacitance to the dielectric constant. The deviation from Curie-Weiss law is observed for almost all the samples. The data in the reciprocal dielectric constant graph (1/έ-T) was fitted with a straight line for $T > T_m$ and the Curie-Weiss temperature (T_{CW}) was estimated from the extrapolation of fitted line. The Burn's temperature T_B is determined from 1/έ-T curve. It refers to the temperature below which 1/έ is non-linear function of T. T_B signifies cross-line between soft mode and order-disorder dynamics. When the temperature decreases below T_B, polar nanoregions appear and the displacive-type soft mode is overdamped. The Curie-Weiss law becomes invalid within the temperature range of T_m-T_B. The difference $\Delta T_m = T_m - T_B$ is used to estimate deviation of system from classical Curie-Weiss behavior as earlier has been discussed by K. Datta et al [36]. In general, T_B rises with doping concentration. However, in present attempt, T_B is found to be decreasing with increase doping level suggest rise of structural ambiguity near phase transition due to MPB. Non-zero values of ΔT_m suggest relaxation near phase transition and it gives rise the broadening of έ-T. Extend of deviation is decreasing near MPB and it further increasing for $x \geq 0.27$. For quantitative measurement of diffuseness, the diffuseness coefficient (γ) is determined by fitting the data to the modified Curie-Weiss law (given by the equation $\frac{1}{\varepsilon_r} - \frac{1}{\varepsilon_m} = c(T - T_m)^{\gamma}$). The diffusive coefficient is decreasing at MPB region from 1.8 to 1.2 and suddenly rise to 2.01 at x = 0.28 (FIG 10). Both results clearly indicate that extend of both relaxation and diffuseness reduced at MPB.

The dielectric constant shows a little independence of frequency at low temperature. But at high temperature, frequency dependence behaviors are observed the dielectric constant rapidly decreasing with increasing frequency. The increase in dielectric constant at low frequency and high temperature is attributed to the oxygen vacancy effect arises due to the composition fluctuation due to A-site ions (Bi^{3+}, Na^{+} , Sr^{2+}) pronounced at high temperature[37].

Dielectric loss is found anomalies near MPB region; the sample with composition x=0.24 show weak frequency dispersion and relaxation before phase transition. However for x=.0.25 onwards relaxation is observed around 300^{0}C. The relaxation anomaly is prominent at 10 KHz frequency, while disappear with rise in frequency. It is not observed for x = 0.28. This attributes to conductance due to mobile charge carriers at low frequency and high temperature.

IV Conclusion

(1-x) NBT-xST (x=0-0.30) solid solution are synthesized by novel hydrothermal-combustion route. X-ray diffraction study confirms the existence of MPB (rhombohedral-pseudocubic) by co-existance of (202), (002), (122) and (112) peaks at x = 0.25-0.26. To investigate dielectric and local structural distortion near MPB details study (1-x) NBT-xST ($SrTiO_3$) (x=0.24-0.28) composition are performed by dielectric permittivity and RAMAN spectroscopy. XRD confirms complete diffusion of cubic phase of ST in NBT with formation of solid solution. RAMAN spectra exhibit appearance of new vibration modes at A and B-site by splitting of peaks in NBT-ST at MPB (x=0.25-0.26), which was obtained for x < 0.25 and disappeared at x > 0.26 onwards. It indicates short range ordering of A-site cations (Bi/Na/Sr) and B-site (TiO_6 octahedral distortion). Dielectric data as a function of temperature show lower shift of dielectric transition temperature from 360^{o}C to 160^{o}C near MPB. The broadening of dielectric peak with deviation from curie-weiss law proves dielectric dispersion near MPB region of NBT-ST. The origin of MPB is result of local imbalance due to chemical inhomogeneity and short range disordering. The induce strain-charge disparity influence dielectric behaviour.

V Acknowledgement:

S.S. wants to acknowledge UGC New Delhi for providing financial assistance through MANF Fellowship. The S.A.A. and P.K. wants to acknowledge the financial support from DST New Delhi, India under project of SR/FTP/PS-106/2009 (G) and UGC under MRP F.N. 41-871/2012.

VI REFERECES

[1] I. Levin, I. M. Reaney, E-M. Anton, W. Jo, J. Rodel, J. Pokorny, L.A. Schmitt, H-J. Kleebe, M. Hinterstein and J. L. Jones, " Local structure, pseudosymmetry, and phase transition in $Na_{1/2}Bi_{1/2}TiO_3$",*Physical Review B 87*, 024113 (2013). DOI 10.1103/PhysRevB.87.024113.

[2] D. Xiao, D. Lin, J. Zhu and P. Yu, "Investigation on the design and synthesis of new system of BNT-based lead free piezoelectric ceramics", *Journal of Electroceramics* 16, 271 (2006). DOI 10.1007/s10832-006-9863-7.

[3] V. Shuvaeva, D. Zekira and A. Glazer, " Local structure of the lead free relaxor ferroelectric $K_xNa_{(1-x)}Bi_{0.5}TiO_3$,*Physical Review B* 71, 174114 (2005). DOI 10.1103/PhysRevB.71.174114

[4] T. Takenaka, K. I. Maruyama and K. Sakata "$(Bi_{1/2}Na_{1/2})TiO_3$-$BaTiO_3$ System for Lead-Free Piezoelctric Ceramics", *Journal of Japanese Applied Physics* 30, 2236 (1991). DOI 10.1143/JJAP.30.2236.

[5] Y. Hiruma, Y. Imai, Y. Watanabe, H. Nagata and T. Takenaka, "Large electrostrain near the phase transition temperatureof $(Bi_{0.5}Na_{0.5})TiO_3$-$SrTiO_3$ ferroelectric ceramics" *Applied Pysics Letters* 92, 262904 (2008). DOI 10.1063/1.2955533.

[6] S. Park and K. Hong, " Variation of structure and dielectric properties on substituting A-site cations for Sr^{2+} in $(Na_{1/2}Bi_{1/2})TiO_3$",*Journal of Material Research* 12, 2152 (1997).DOI 10.1557/JMR.1997.0288.

[7] T. Wang, H. DU and X. SHI, " Dielectric and ferroelectric properties of (1-)$Na_{0.5}Bi_{0.5}TiO_3$-x$SrTiO_3$ Lead –free piezoceramic system" *Journal of Physics: Conference Series* 152, 012065 (2009). DOI 10.1088/1742-6596/152/1/012065.

[8] W. Krauss, D. Schutz, F. Mautner, A. Feteira and K. Reichmann, " Piezoelectric properties and phase transition temperatures of the solid solution of (1-x) $(Bi_{0.5}Na_{0.5})TiO_3$-x$SrTiO_3$",*Journal of the European Ceramic Society* 30, 1827 (2010). DOI 10.1016/j.jeurceramsoc.2010.02.001.

[9] S. Gorfman, A. Glazer, Y. Noguchi, M. Miyayama, H. Luo and P. Thomas, "Observation of a low symmetry phase in $Na_{0.5}Bi_{0.5}TiO_3$ crystal by optical birefringence microscopy"*Journal of Applied Crystallography* 45, 444 (2012). DOI 10.1107/S0021889812008217.

[10 S. Trujillo, J. Kreisel, Q. Jiang, J. Smith, P. Thomas, P. Bouvier and F. Weiss, "The high pressure behaviour of Ba-doped investigated by RAMAN spectroscopy",*Journal of Physics: Condense Matter* 17, 6587 (2005). DOI 10.1088/0953-8984/17/41/027.

[11] D. Rout, K. Moon, J. Park and S. Kang, " High Temperature X-Ray diffraction and Raman scattering studies , of Ba-doped ($Na_{0.5}Bi_{0.5})TiO_3$"*Current Applied Physics* 13,1988 (2013). DOI 10.1016/j.cap.2013.08.016.

[12] Y. Li, W. Chen, J. Zhou, Q.Xu, H. Sun and R. Xu, " Dielectric and piezoelectric properties of lead-free ($Na_{0.5}Bi_{0.5})TiO_3$ –$NaNbO_3$ceramics",*Material Science & Engineering B* 112,5 (2004).DOI 10.1016/j.mseb.2004.04.019.

[13] B.N.Rao, R Dutta, S S Chandrashekaran, D K Mishra, V Sathe, A. Senyshen, and R. Ranjan, “Local structural disorder and its influence on the average global structure and polar properties in $Na_{0.5}Bi_{0.5}TiO_3$”,*Physics Review B* 88, 224103-14 (2013). DOI: dx.doi.org/10.1103/PhysRevB.88.224103.

[14] X. Wang,H. Chan and C. Choy, “$(Bi_{1/2}Na_{1/2})TiO_3$-$Ba(Cu_{1/2}W_{1/2})O_3$ Lead-free piezoelectric ceramics” *Journal of American Ceramic Society* 86,1809 (2003). DOI: 10.1111/j.1151-2916.2003.tb03562.x.

[15] V. Dorcet, G. Trolliard and P. Boullay, “The structural origin of the antiferroelectric properties and relaxor behavior of $Na_{0.5}Bi_{0.5}TiO_3$” *Journal of Magnetism and Magnetic Materials*321, 1758 (2009) DOI: 10.1016/j.jmmm.2009.02.013.

[16] E. Aksel, J. Forrester, B. Kowalski, J. Jones and P. Thomes, “Phase transition sequence in sodium bismuth titanate observed using high-resolution x-ray diffraction”, *Applied Physics Letters* 99, 222901 (2011). DOI: 10.1063/1.3664393.

[17] S. Zhang, A. Kounga, E. Aulbach and Y. Deng, “ Temperature-Dependent Electrical Properties of $0.94Bi_{0.5}Na_{0.5}TiO_3$-$0.06BaTiO_3$ Ceramics”,Journal of American Ceramic Society 91, 3950 (2008). DOI: 10.1111/j.1551-2916.2008.02778.x.

[18] Y. Hiruma, K. Yoshii, H. Nagata and T. Takenaka, “Phase transition temperature and electrical properties of $Bi_{1/2}Na_{1/2}TiO_3$-$(Bi_{1/2}A_{1/2})TiO_3$ (A=Li and K) lead-free ferroelectric Ceramics”,*Journal of Applied Physics* 103, 084121 (2008). DOI: 10.1063/1.2903498

[19] R. Ranjan, R. Garg, V. kothai, A. Agrawal, A. Senyshyn and H. Boysen, “Phases in the $(1-x)Na_{0.5}Bi_{0.5}TiO_3$–$(x)CaTiO_3$system”’ *Journal of Physics: Condens Matter* 22, 075901 (2010). DOI:10.1088/0953-8984/22/7/075901.

[20] J. Kreisel, A. Glazer, G.Jones, P. Thomas, L. Abello and G. Lucazeau, “An x-ray diffraction and Raman spectroscopy investigation of A-site substituted perovskite compounds:the $(Na_{1-x}K_x)_{0.5}Bi_{0.5}TiO_3$ ($0 \leq x \leq 1$) solid solution”,*Journal of Physics: Condens. Matter* 12, 3267 (2000). DOI:10.1088/0953-8984/12/14/305.

[21] Ji. Hao, W. Bai, W. Li, B. Shen and J. Zhai, “Phase transitions, relaxor behavior, and electrical properties in (1-x)$(Bi_{0.5}Na_{0.5})TiO_3$–x$(K_{0.5}Na_{0.5})NbO_3$lead-free piezoceramics”,*Journal of Material Research* 27, 2943 (2012). DOI: 10.1557/jmr.2012.328.

[22] F. Gao, X. Dong, C. Mao, H. Zhang, Fei Cao and G. Wang, “Poling temperature tuned electric-field-induced ferroelectric to antiferroelectric phase transition in $0.89Bi_{0.5}Na_{0.5}TiO_3$-$0.06BaTiO_3$-$0.05K_{0.5}Na_{0.5}NbO_3$ceramics” ,Journal of Applied Physics 110, 094109 (2011). DOI: 10.1063/1.3660283.

[23] K. Sakata and Y. Masuda, “Ferroelectric and antiferroelectric properties of $(Na_{0.5}\ Bi_{0.5})$Ti03- $SrTiO_3$, solid solution ceramics”, *Ferroelectrics* 7, 347 (1974). DOI:10.1080/00150197408238042.

[24] D. Rout, K. Moon, S. Kang and I. Kim, “Dielectric and Raman scattering studies of phase transitions in the (100-x) $Na_{0.5}\ Bi_{0.5}\ TiO_3$ – x $SrTiO_3$ system” *Journal of Applied Physics* 108,84102 (2010). DOI:10.1063/1.349078.

[25] P. Jaita , A. Watcharapasorn and S. Jiansirisomboon, “Investigation of a new lead-free $Bi_{0.5}(Na_{0.40}K_{0.10})TiO_3$-$(Ba_{0.7}Sr_{0.3})TiO_3$piezoelectric ceramic” *Nanoresearch letters* 17, 24 (2012).

[26] X. Wang, S. Choy, X. Tang and H. Chan "Dielectric behavior and microstructure of,,$Bi_{1/2}Na_{1/2}TiO_3$-$Bi_{1/2}K_{1/2}TiO_3$–$BaTiO_3$ lead-free piezoelectric ceramics", *Journal of Applied Physics* 97, 104101 (2005). DOI: 10.1063/1.1890453.

[27] M. Yoon, Y. Lee and S. Ur, "Effects of co-doped CaO/MnO on the piezoelectric/dielectric properties and phase transition of lead-Free$(Bi_{0.5}Na_{0.5})_{0.94}Ba_{0.06}TiO_3$ piezoelectric ceramics", *Journal of electroceramic* 23, 564 (2009). DOI 10.1007/s10832-008-9548-5.

[28] O. Muller and R. Roy, "The Major Ternary Structural Families", *Springer,New York*, , p. 221 (1974).

[29] F.S. Galasso, "Perovskites and High Tc Superconductors", *New York Gordon and Breach* (1990).

[30] S. Shanmuga Sundari, B. Kumar and R. Dhanasekaran,"Structural, Dielectric, Piezoelectric and Ferroelectric Characterization of NBT-BT Lead-Free Piezoelectric Ceramics" *IOP Conf. Ser.: Mater. Sci. Eng.* ,43, 012010 (2013).

[31] J. Kreisel, A. Glazer, G. Jones, P.A. Thomas, L. Abello and G. Lucazeau, "An x-ray diffraction and Raman spectroscopy investigation of A-site substituted perovskite compoundsthe $(Na_{1-x}K_x)_{0.5}Bi_{0.5}TiO_3$ ($0\leq x\leq1$) solid solution", *J. Phys: Condense Matter.* 12, 3267 (2000). DOI:10.1088/0953-8984/12/14/305.

[32] B. Parija, S. Rout, L. Cavalcante, A. Simoes, S. panigrahi, E. Longo and N. Batista, "Structure, microstructure and dielectric properties of 100−x$(Bi_{0.5}Na_{0.5})TiO_3$−x[$SrTiO_3$] composites ceramics" *Applied Physics A* 109, 715 (2012). DOI 10.1007/s00339-012-7105-1.

[33] S. Tripathy, K. Mishra, S. Sen and D. Pradhan, "Dielectric and Raman Spectroscopic Studies of $Na_{0.5}Bi_{0.5}TiO_3$–$BaSnO_3$ Ferroelectric System",*Journal of American Ceramic*

Society ,9 (2014). DOI: 10.1111/jace.1283.

[34] J. B. Babu, M.He,D.F. Zhang, J. Hao, "Enhancement of ferroelectric properties of $Na_{1/2}Bi_{1/2}TiO_3$-$BaTiO_3$ single crystals by Ce dopings"*Applied Physics Letters*, 31, 102901 (2007). DOI: 10.1063/1.2709917.

[35] Ch. S. Devi, G.S.Kumar and G. Prasad. "Control of ferroelectric phase transition in nano particulate NBT–BT based Ceramics" ,*Material Science and engineering B*,178, 283 (2013). DOI: 10.1016/j.mseb.2012.12.001.

[36] K. Datta, P. Thomas, K. Roleder, "Anomalous phase transitions of lead-free piezoelectric $xNa_{0.5}Bi_{0.5}TiO_3-(1-x)BaTiO_3$ solid solutions with enhanced phase transition temperatures", *Physical Review B* 82, 224105 (2010). DOI:10.1103/PhysRevB.82.224105.

[37] S. Bhandari, N. Sinha, G. Ray and B. Kumar, "Flux growth of lead free $(Na_{0.5}Bi_{0.5})TiO_3$–$(K_{0.5}Bi_{0.5})TiO_3$ ferroelectric single crystals and their characterization",Cryst. Eng Comm 16, 4459 (2014). DOI: 10.1039/c4ce00249k.

Figure Caption:

1. FIG 1: (a) XRD of NBT-ST at different composition of ST (b & c) magnified view of additional peaks.
2. FIG 2:. Rietveld refinement of NBT system.
3. FIG 3: Gaussian Fitting of (202) peak.
4. FIG 4: SEM images of (a) Pure NBT and (b)0.74NBT-0.26ST solid solution
5. FIG 5: EDX (a) Pure NBT and (b)0.74NBT-0.26ST solid solution Room temperature.
6. FIG 6: RAMAN spectra of NBT-ST with different composition. Inset shows magnified view of RAMAN anomaly.
7. Fig 7: Temperature dependent RAMAN spectra of NBT-ST system during heating and cooling cycle.
8. FIG 8: έ-T and tanδ-T curve of NBT-ST system.
9. FIG 9: Reciprocal dielectric 1/έ verses Temperature curve.
10. FIG 10: Modified Currie- Weiss Law.

Table caption:

1. Table 1: Elemental distribution of NBT based system by EDX

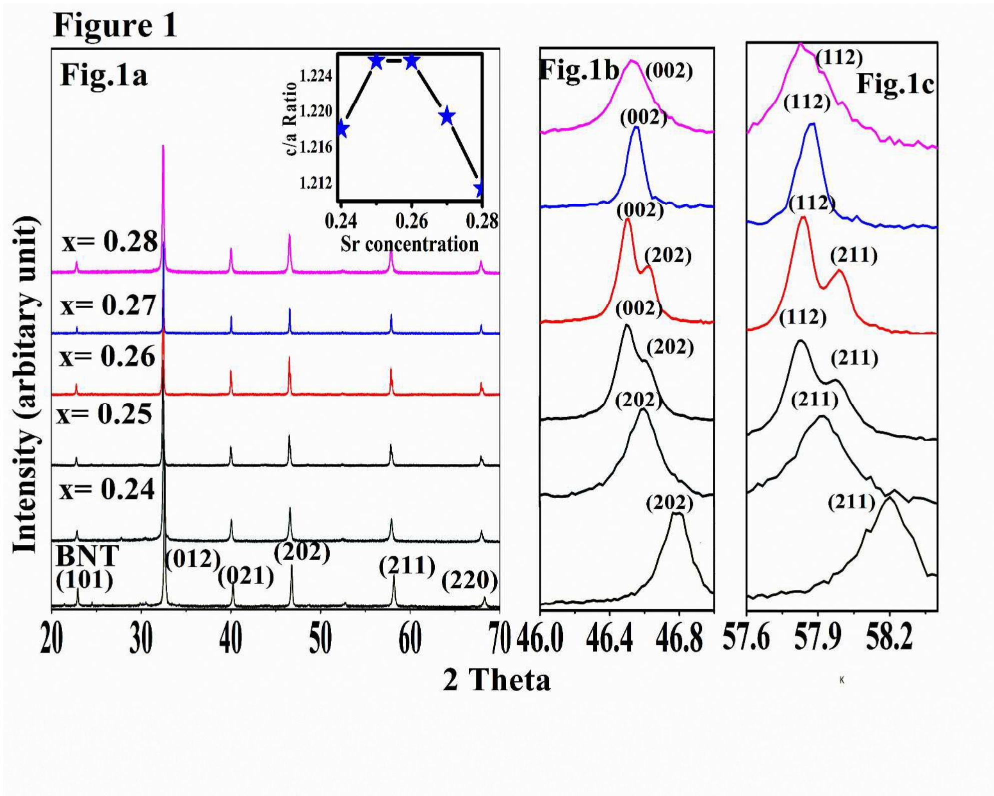

(a) XRD of NBT-ST at different composition of ST (b & c) magnified view of additional peaks.
318x254mm (299 x 299 DPI)

Figure 2

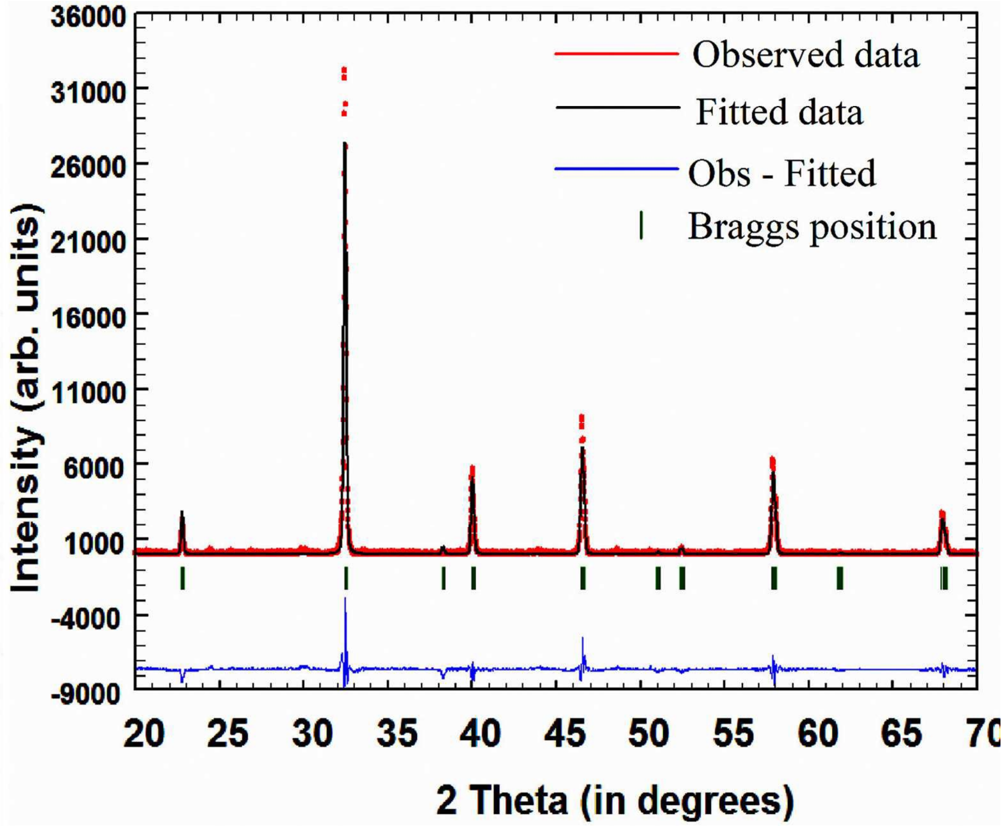

Rietveld refinement of NBT system.
114x108mm (299 x 299 DPI)

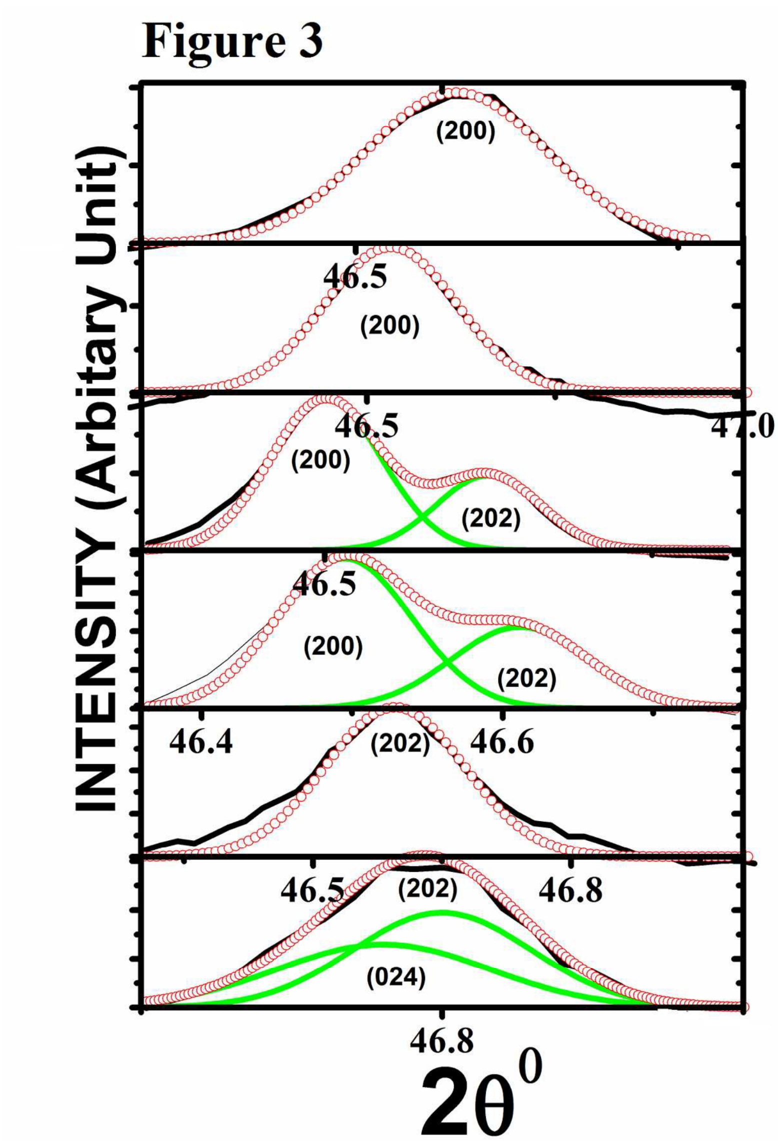

Gaussian Fitting of (202) peak
426x595mm (96 x 96 DPI)

Figure 4

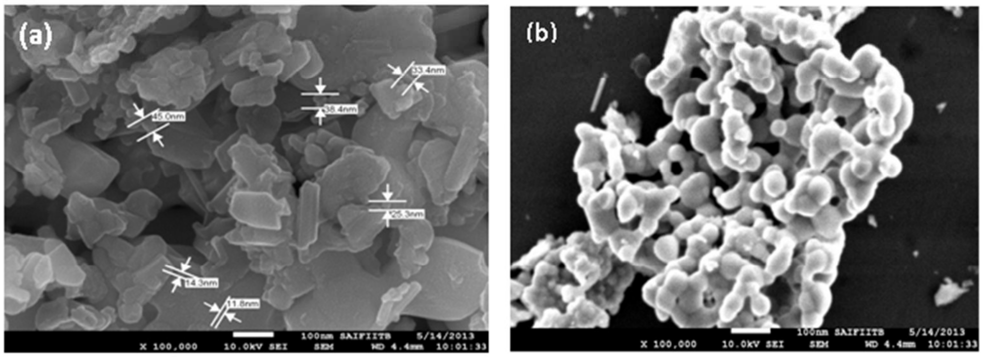

SEM images of (a) Pure NBT and (b)0.74NBT-0.26ST solid solution
184x86mm (96 x 96 DPI)

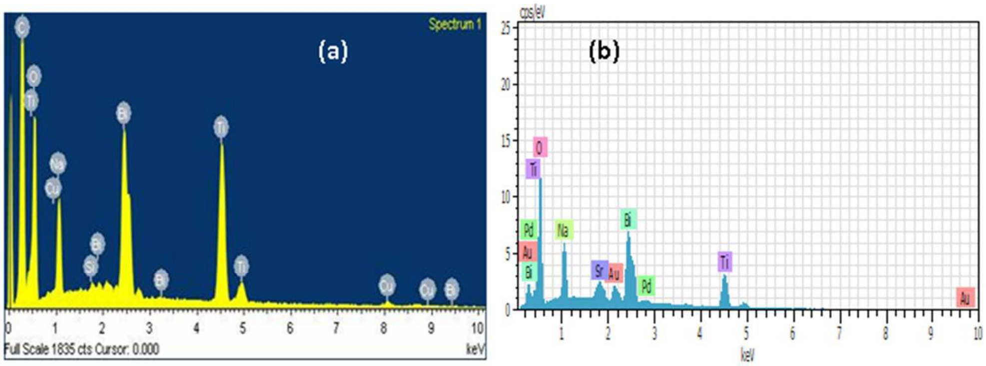

EDX (a) Pure NBT and (b)0.74NBT-0.26ST solid solution Room temperature.
182x67mm (96 x 96 DPI)

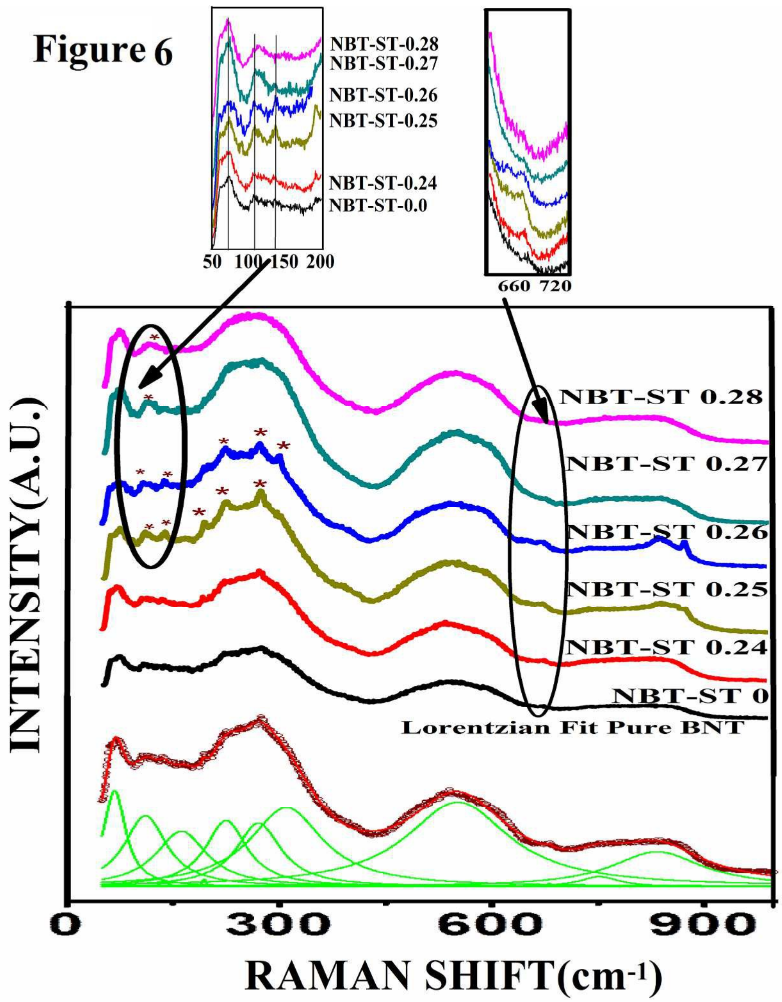

RAMAN spectra of NBT-ST with different composition. Inset shows magnified view of RAMAN anomaly.
635x635mm (96 x 96 DPI)

Figure 7

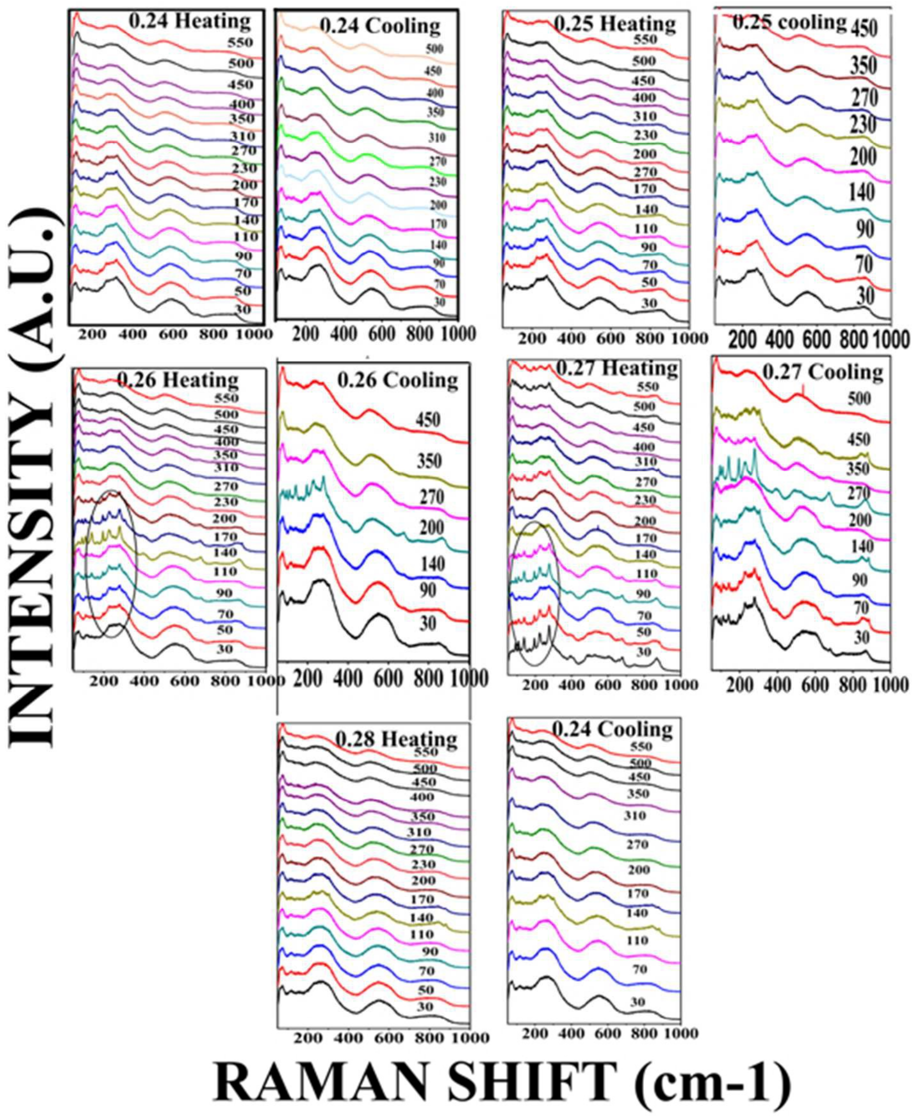

Temperature dependent RAMAN spectra of NBT-ST system during heating and cooling cycle.
158x200mm (96 x 96 DPI)

Figure 8

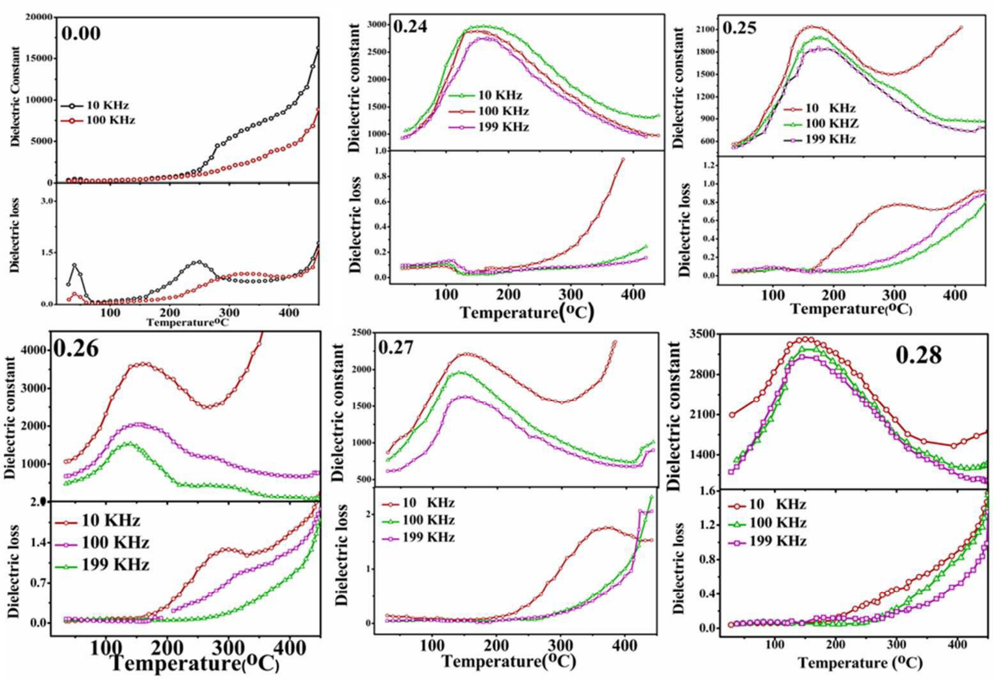

έ-T and tanδ-T curve of NBT-ST system.
270x206mm (96 x 96 DPI)

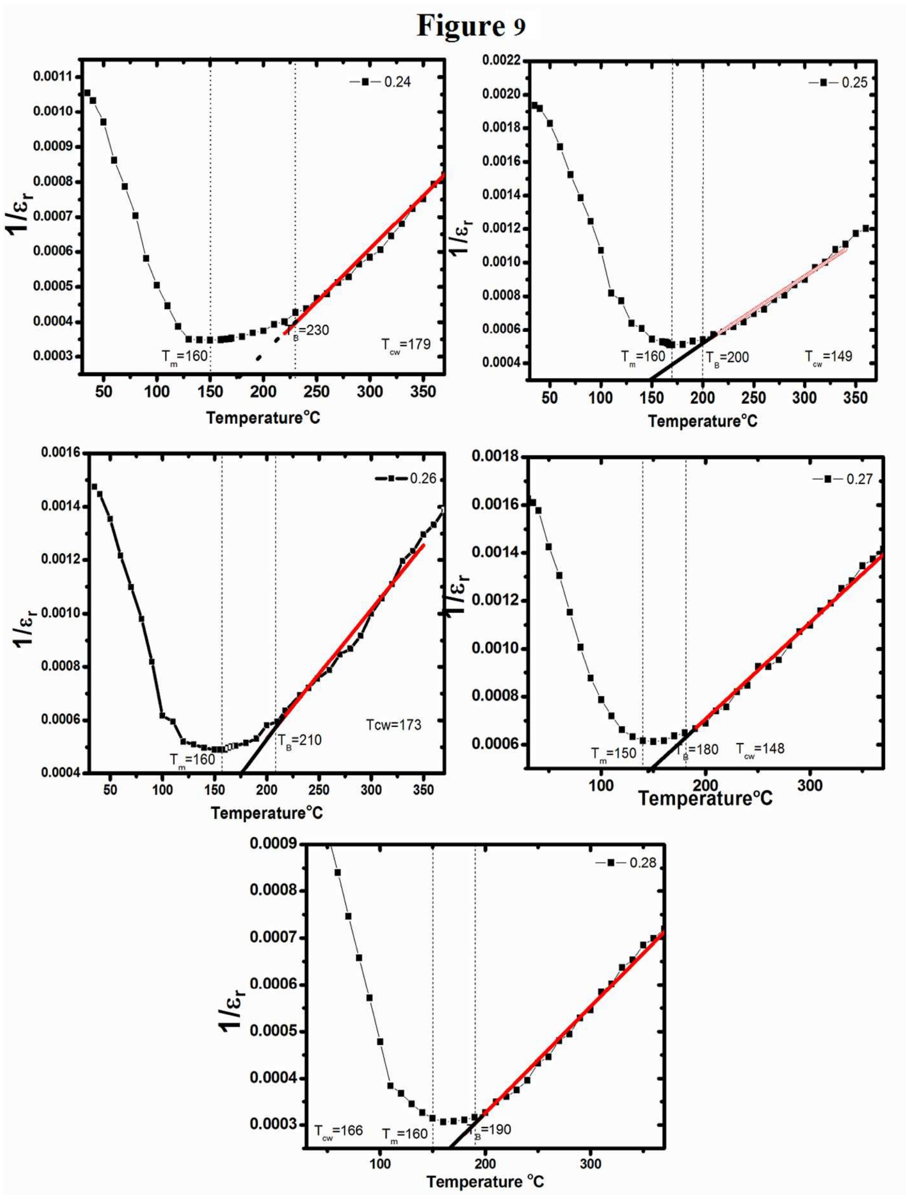

Reciprocal dielectric 1/έ verses Temperature curve.
361x476mm (96 x 96 DPI)

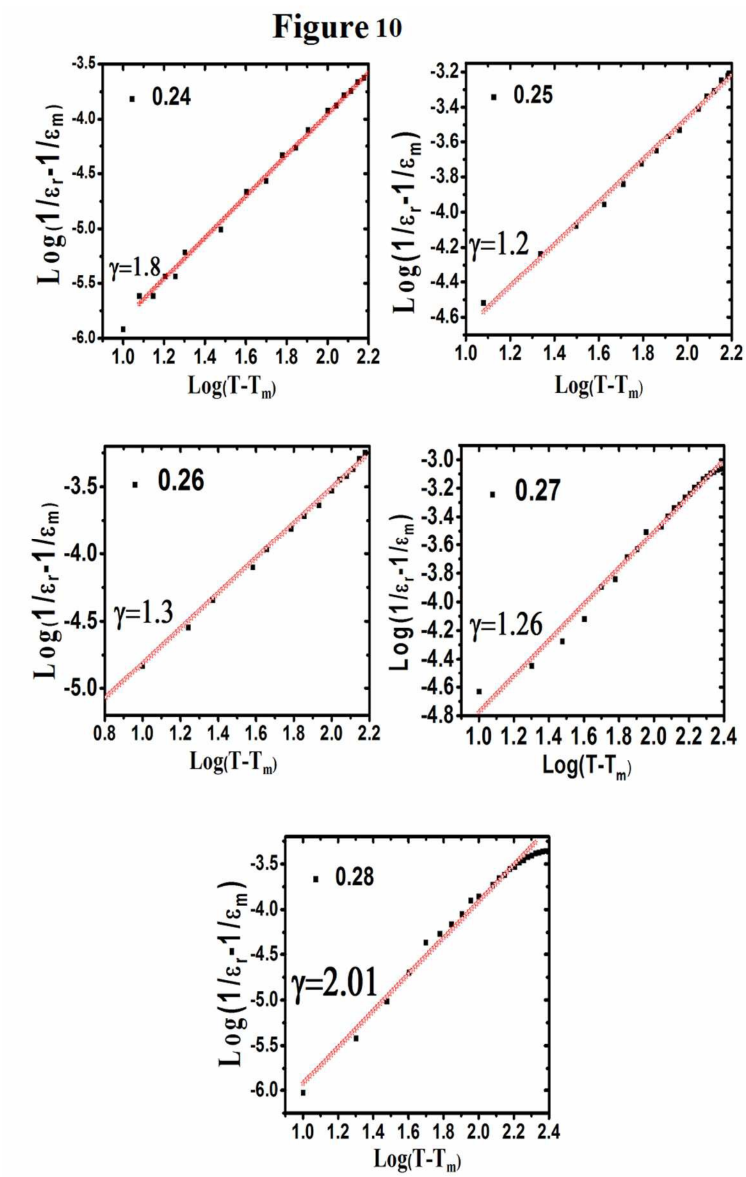

Modified Currie- Weiss Law.
285x436mm (96 x 96 DPI)

Table 1: Elemental distribution of NBT based system by EDX

Sr. No	$Bi_{0.5}Na_{0.5}TiO_3$		0.74($Bi_{0.5}Na_{0.5}TiO_3$)-0.26(SrTiO3)	
	Element	Atomic %	Element	Atomic %
1	Bi	2.38	Bi	6.54
2	Na	3.77	Na	11.11
3	Ti	7.67	Ti	24.63
4	O	34.27	O	54.31
5	Si	0.18	Sr	2.05
6	Cu	2.09	Au	1
7	C	51.02	Pd	0.36